

Post-compression of high energy terawatt-level femtosecond pulses and application to high order harmonic generation

Ondřej Hort, Antoine Dubrouil, Amélie Cabasse, Stéphane Petit, Eric Mével, Dominique Descamps, and Eric Constant

*Univ. Bordeaux, CEA, CNRS,
CELIA (Centre Lasers Intenses et Applications)
UMR5107, F-33400 Talence, France* and*

O. Hort current address: Photonics Institute, Vienna University of Technology, Gusshausstrasse 27-29, A-1040 Vienna, Austria

We perform a post-compression of high energy pulses by using optical-field ionization of low pressure helium gas in a guided geometry. We apply this approach to a TW chirped-pulse-amplification based Ti:Sapphire laser chain and show that spectral broadening can be controlled both with the input pulse energy and gas pressure. Under optimized conditions, we generate 10 fs pulses at TW level directly under vacuum and demonstrate a high stability of the post compressed pulse duration. These high energy post-compressed pulses are thereafter used to perform high harmonic generation in a loose focusing geometry. The XUV beam is characterized both spatially and spectrally on a single shot basis and structured continuous XUV spectra are observed.

PACS numbers: (140.7090), (190.4160), (260.7200), (320.5520), (320.7110).

Keywords: Ionization-induced spectral broadening, high energy post-compression High harmonic generation, Ultrashort laser pulses, Terawatt femtosecond laser

I. INTRODUCTION

Few-cycle intense laser pulses are now routinely generated with pulse energy at the mJ level and they are often used to generate high order harmonics and attosecond pulses [1]. The fundamental pulse energy impacts strongly the number of photons in the extreme ultraviolet (XUV) pulse therefore lot of effort is currently devoted to increasing the energy of few cycle laser pulses [2]. Several approaches have been proposed like optical-parametric chirped-pulse amplification (OPCPA) [3, 4], Kerr effect based post-compression in a gas-filled capillary [5, 6] or gas-filled planar waveguides [7, 8] and filamentation [9–11].

While OPCPA gives access to multi-TW short pulses, the picosecond pump design stays very sophisticated and to date there is just one operated laser system able to deliver few-cycle pulses with few tens of milijoules [12]. The Kerr effect based post-compression is compatible with state-of-the-art Ti:Sapphire laser chain, the output pulse energy is however limited to few mJ by the low critical peak power of self focusing since high gas pressure (few bars) is required for Kerr induced self phase modulation.

As optical-field ionization of gas is highly nonlinear, large spectral broadening can be achieved with low gas pressure and allows to post-compress femtosecond pulses at high energy level. Thus we designed a post-compression technique that uses helium ionization in a capillary to shorten pulse duration and use it on 55 fs 75 mJ pulses (TW level) and obtained 10 fs duration TW pulses with homogeneous beam profile. This technique was first reported in [13], where a small fraction of the output pulse energy was compressed. Here, we study the

temporal compression of the entire energy of the spectrally broadened pulse and characterized the shot to shot stability of the pulse duration. More specifically, the impact of the initial pulse energy and the helium pressure on the pulse broadening as well as the stability of the re-compressed pulse duration is investigated.

To confirm the suitability of the pulses for high field physics, we use these post-compressed pulses to generate high order harmonics in a loose focusing geometry in a regime of high ionization level. The XUV pulses are characterized spatially and spectrally and the high output photon flux is compatible with single shot characterization. The XUV beam exhibits clear spatial and spectral structures and spectrally gets continuous when the HHG is performed with 10 fs post-compressed TW pulses.

II. EXPERIMENTAL SETUP

We use a Ti:Sapphire chirped-pulse-amplification-based laser chain delivering pulses of 75 mJ and 55 fs pulse duration (FWHM) at a repetition rate of 10 Hz. The beam, propagating under vacuum, is focused by a 3 m focal length spherical mirror into a 40 cm long glass capillary with inner diameter of 420 μm (fig. 1). The laser beam focal spot size and position was adjusted to favor monomode coupling $\frac{w_0}{r_{cap}} = 0.645$ [14] and monomode guiding was ensured by observing the beam profile in the far field after the capillary. Helium gas was injected in this capillary at controlled pressure via a side hole and the gas was leaking to the vacuum chambers via both ends of the capillary. At high laser intensities ($> 10^{15} \text{ W/cm}^2$), the laser pulse ionized the helium gas which broadens the pulse spectrum through self phase modulation induced by fast evolution of free-electron density.

* ondrej.hort@tuwien.ac.at

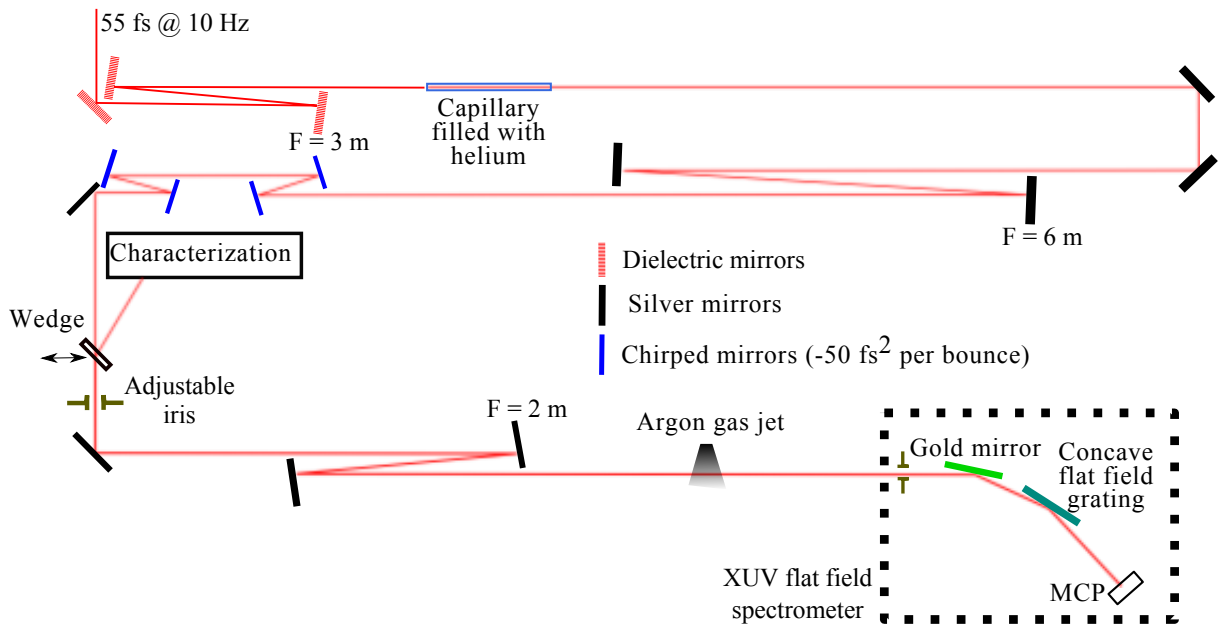


Figure 1. (color online) Experimental setup of the post-compression and high harmonic generation. The setup is under vacuum and allows both post-compression (helium filled capillary and chirped mirrors) of the TW pulses and high order harmonic generation. High order harmonics are characterized on a single-shot basis with a flat-field spectrometer with high spatial and spectral resolution.

Since optical-field ionization is very fast and highly nonlinear, large spectral broadening can be achieved with low gas pressure (few mbar) in comparison with Kerr induced self phase modulation (few bar) [13, 15–17]. After the capillary, a 6 m focal length spherical mirror collimates the output beam to a size of $w = 10$ mm (radius at $I_{max}/2e^2$). After this collimating mirror (diameter of 40 mm) only the fundamental mode is selected as the other modes are more divergent. By injecting 75 mJ pulses at the capillary entrance, the transmitted energy without helium gas in the capillary was 30 mJ (after the collimating mirror and chirped mirrors). This rather low coupling efficiency was likely due to quasi-flat top spatial profile and corresponding wavefront of the injected beam (standard characteristic for high energy CPA laser chains), losses due to the gas injection hole and capillary roughness. The coupling efficiency could be improved with a proper beam shaper and higher optical quality of the capillary.

To compensate the chirp of the pulse acquired during the spectral-broadening process in the capillary, 4 chirped mirrors (inducing a -50 fs² GVD per reflection) are located under vacuum after the collimation.

We characterize the output pulse with a single-shot spectrometer and a single-shot autocorrelator located in air. A fraction of the laser beam is reflected by a mobile beam sampler (uncoated silica wedge), exits the vacuum chamber via a 3 mm thick BK7 window and is sent for temporal and spectral characterization by a single-shot autocorrelator and a spectrometer. To compensate the dispersion of the window and the air we placed 4 addi-

tional chirped mirrors (-50 fs² each) and a 1 mm silica plate in front of the autocorrelator. In this way, the measured pulse duration was identical to the pulse duration under vacuum and this characterization allowed us to study the impact of the input parameters (helium pressure, pulse energy).

The beam sampler can be removed to use the beam for HHG. The beam is focused with a 2 m focal length spherical mirror in a pulsed argon gas jet located 5 cm before the focus. Note that in this configuration high harmonics are generated in a loose focusing configuration at high intensity of 5×10^{14} W/cm², which is above the saturation level of argon (2.5×10^{14} W/cm²). An adjustable iris permits to control the infrared intensity and the beam size in the generating medium to maximize the XUV signal. The gas jet is a pulsed valve (Parker Series 9) with 250 μ m inner diameter nozzle, 400 μ s opening time and it is operated with an argon backing pressure of 4.5 bar. The setup can also be used for comparison with 55 fs pulses by evacuating the helium gas in the capillary.

The harmonics are characterized by a flat-field XUV spectrometer. The 500 μ m vertical entrance slit of the spectrometer is located 119 cm after the jet. The spectrometer consists in a Hitachi cylindrical concave gold grating with 1200 grooves per mm used at 87° grazing incidence angle. The concave grating images the slit with a magnification of 1 in the horizontal (spectral) dimension on a dual microchannel plate (MCP) detector equipped with a phosphor screen and observed with a 12 bit CCD. In the vertical dimension, the beam propagation is not affected by the grating allowing us to observe the spatial

profile of the XUV beam in the far field. The XUV photon flux was high enough to characterize the harmonic beam with both spectral and spatial resolution on a single shot basis.

III. EXPERIMENTAL RESULTS

A. Spectral broadening in the helium gas filled capillary

Here we study the spectrum of the IR pulses at the output of the capillary as a function of backing helium pressure and input pulse energy. As the high intensity infrared laser pulse propagates through the helium-filled capillary and ionizes the gas, its spectrum changes significantly even with a low gas pressure. Both a broadening and a blue shift of the spectra are observed.

Figure 2 shows the evolution with helium pressure of the output pulse spectra. Even 1 mbar of helium pressure is sufficient to significantly broaden the incident pulse spectrum (figure 2).

Both a blue shift and a spectral broadening result from a time-dependent optical refractive index of the gas medium in the capillary as it is dependent on the free-electron density induced by the medium ionization. Time dependent-phase accumulation during propagation in the capillary results in a shift of the instantaneous frequency that can be described in a 1D approach as $\omega(t) = -\frac{d}{dt} \left(-\omega_0 t + L \frac{2\pi}{\lambda_0} \sqrt{1 - \frac{n_e(t)}{n_c}} \right)$ [13, 15, 16] where $n_e(t)$ denotes time-dependent free-electron density and L the length of the capillary.

With gas injected in the capillary, the output spectrum broadens and splits into several peaks. The red-side peak position is constant and peaks around 830 nm. The blue-side peak position experiences a blue shift increasing with pressure until a maximal broadening is reached (between 7 and 10 mbar; see fig. 2) and the spectral width increases rapidly with pressure. At helium pressure higher than 10 mbar, no significant spectral broadening is observed and spectral structures remain mostly unchanged. It can be seen that figure 2 is divided into two regions: 0 to 10 mbar and 10 to 50 mbar respectively. The first region is characterized by a rapid evolution of the central wavelength and the width changes from an initial value of 27 nm to more than 100 nm at 10 mbar of He. The second region exhibits broad spectra whose shape is mainly independent on the helium pressure and most of spectral energy is centered around 800 nm. Later in this section, we will show that the highest peak power output pulses for a given input pulse energy are obtained at the frontier of the two regions i.e. at the maximal broadening pressure threshold.

The spectral broadening is also very dependent on the input pulse energy. Figure 3 shows the output spectra evolution with the input pulse energy for a fixed helium pressure of 7 mbar in the capillary.

We observe that the spectral broadening increases regularly with the pulse energy and a significant broadening was obtained even with 46 mJ of input pulse energy. The observed spectral evolution are similar for both energy and pressure control but both can be interesting as they may have different impact on the output pulse chirp. As the chirp compensation is fixed here by the number of chirped mirrors located under vacuum it was beneficial to have several possibilities of control on the pulse characteristics.

At the highest input energy of 75 mJ and 7 mbar of helium, the output spectrum exhibits a regular shape and a large spectral width (120 nm FWHM) with an output energy as high as 10.9 mJ. In these experimental conditions, the spatial profile of the beam remained uniform and comparable to [13].

B. Duration and energy of the post-compressed pulses

The possibility to obtain short pulses depends both on the spectral width and on the spectral phase. To estimate the shortest pulse duration that could be achieved with the measured spectra shown on figure 2, we performed a Fourier transform of the experimental spectra and plotted the corresponding FWHM duration on figure 4.

The figure shows that shorter pulses can potentially be obtained at high helium pressure. However, above 10 mbar of helium pressure the pulse duration does not significantly change any more and reaches the shortest value of 7.5 fs.

The energy of the output pulses was also measured (after chirped mirrors) as a function of the helium pressure (figure 5). In this way, only the fundamental mode of the beam is selected as high order modes of the capillary are more divergent for the beam line with the effective diameter of 35 mm. Note that the fundamental mode selection is performed before pulse energy measurement. We observed that the pulse energy regularly decrease as the helium pressure increases. This can be understood as part of the pulse energy is coupled in high order modes of the capillary or uncoupled in the capillary and leaking through capillary walls. Both effects leading to optical losses are due to radial gradient of the electron density [16]. Finally, output pulses with energy higher than 10 mJ and significant spectral broadening are achieved for helium pressure around 7 mbar.

In our study, we re-compressed the whole energy of the output pulse in a collimated beam under vacuum. The GVD compensation via chirped mirrors was not adjustable as the number of reflection was limited to 4 reflections and could not be changed easily under vacuum. Nevertheless a proper choice of broadband paired mirrors with compensated GVD oscillations allowed us to re-compress the pulses close to the Fourier limit. The measured post-compressed pulse duration as a function

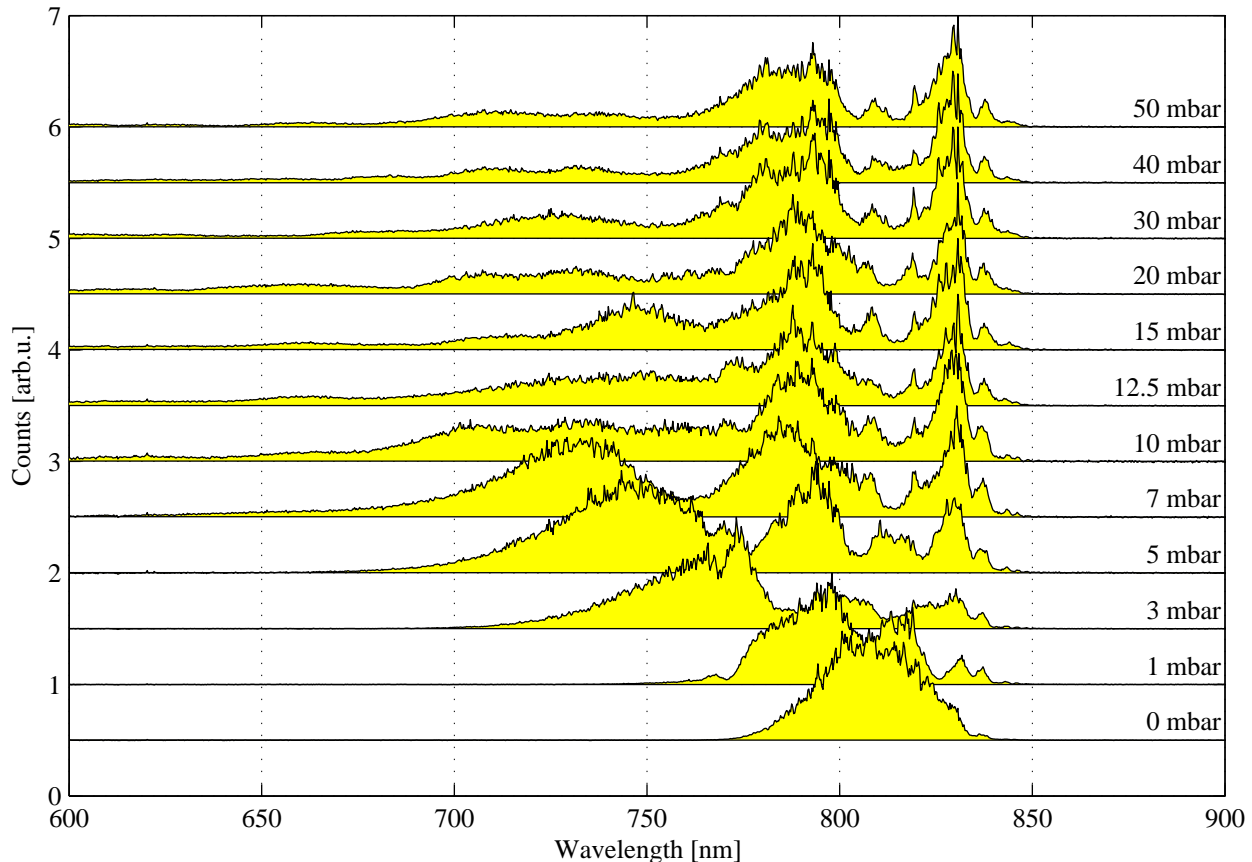


Figure 2. Normalized experimental infrared spectra obtained after guided propagation of the pulse through the capillary for several backing pressure of helium gas injected in the capillary. The incident energy at the entrance of the capillary is 75 mJ. Note that the energy coupled into fundamental mode of the capillary without gas is 30 mJ.

of helium pressure is presented on figure 6. Each point represents the FWHM of a single shot autocorrelation trace. A typical autocorrelation trace can be found in [18]. Figure 6 clearly shows that short pulses can be obtained and their duration can be controlled via pressure tuning between 0 and 10 mbar. The pulse duration drops down to 9.9 fs at 7 mbar and 8.9 fs at 10 mbar considering a factor of 1.49 between the pulse FWHM and autocorrelation FWHM (factor of deconvolution).

One should also note that we achieved a high stability of the output pulse duration. For 10 mbar of the helium pressure the autocorrelation stays around 13.9 fs (inset of figure 6) corresponding to a pulse duration of 9.3 fs after the deconvolution with 3.4 % of RMS stability.

Since high helium pressure ensures large spectral broadening but also decreases output pulse energy, there is a clear trade-off when maximum peak power is pursued. Figure 7 presents peak power of output pulses as a function of helium pressure in the capillary. One can see that the peak power has a maximum between 7 and 10 mbar where it approaches 1 TW. Outside this region, the peak power decreases because, for higher pressure than 10 mbar, the pulse duration stays the same (see figure 6) but the energy drops with pressure (figure 5). For less

than 7 mbar the peak power decrease towards the value of 0.5 TW when the helium pressure is zero.

C. High harmonics generation with post-compressed pulses

The 10 fs post-compressed pulses have been used to generate high order harmonics in a loose focusing geometry with a setup designed for high energy TW pulses [19]. We performed HHG in argon gas jet. Due to the focusing geometry (figure 1) and intensity of the infrared driving pulses, the HHG is performed in the regime of loose focusing and reaches the intensity regime where the argon ionization is significant. XUV spectra were acquired in the far field by a spectrometer with spectral and spatial resolution on the single-shot basis as described in section II.

As a reference, we first acquired an harmonic spectrum without post-compression (without helium in the capillary) and at low intensity ($2.1 \times 10^{14} \text{ Wcm}^{-2}$) by clipping the beam diameter to 10 mm before focusing. Without helium gas in the capillary, the high harmonics are generated with 55 fs pulses (figure 8 (a)) and are

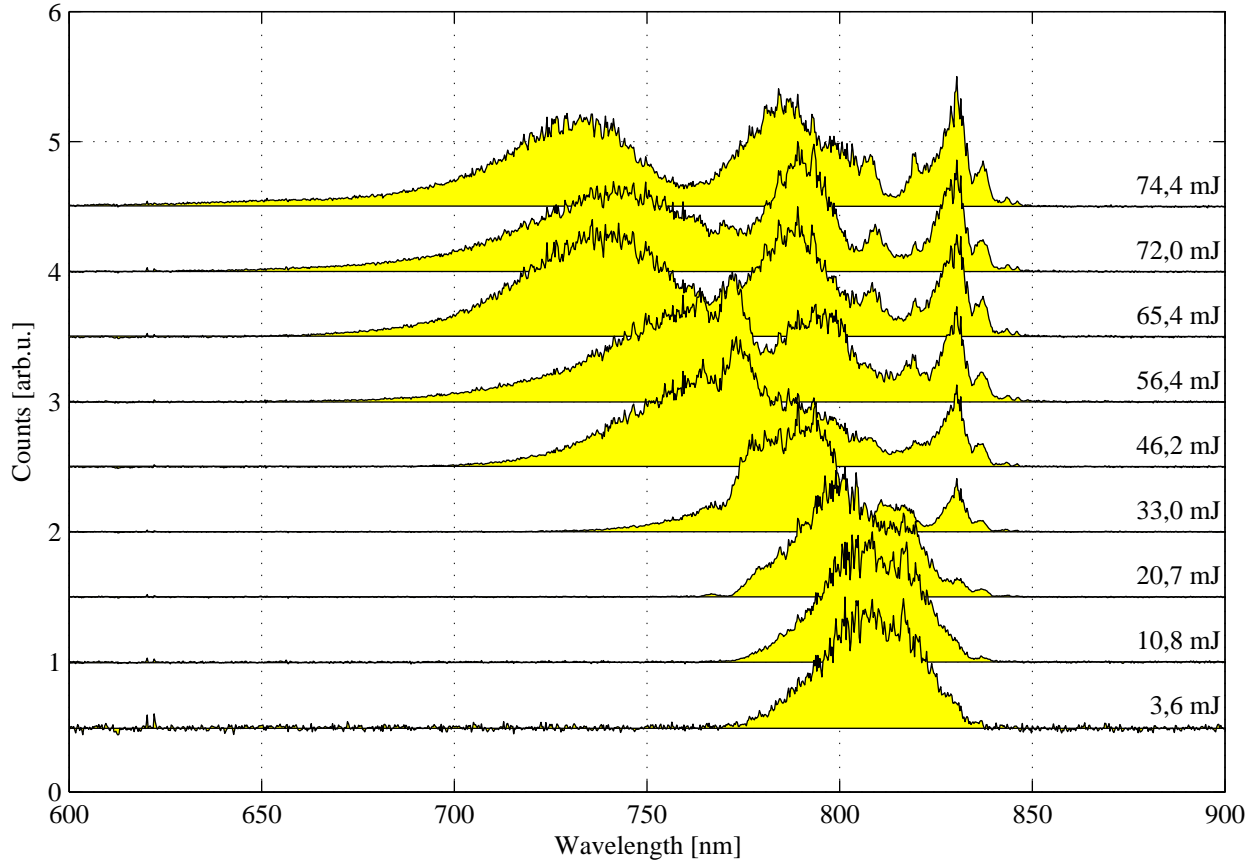


Figure 3. Normalized infrared spectra obtained after guided propagation of the pulse through the capillary for several incident energy of the pulse. Helium pressure in the capillary is 7 mbar.

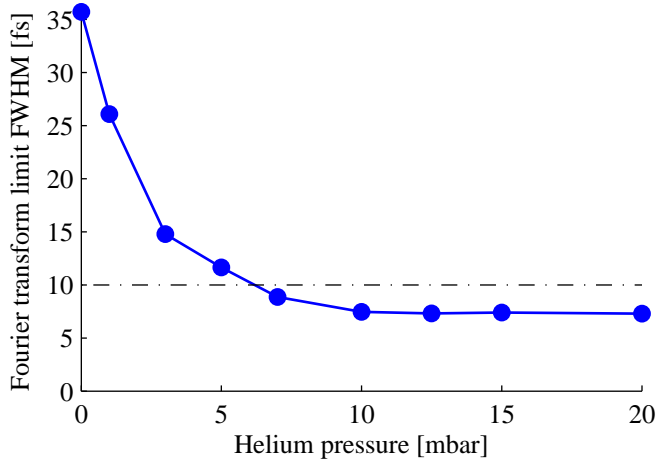


Figure 4. Evolution of the Fourier transform limit output pulse duration as a function of the helium gas pressure in the capillary obtained at an incident energy of 75 mJ.

spatially uniform and symmetric with a cutoff around 50 eV. The spatially resolved harmonics shows ellipses that are attributed to long trajectories and intense spectrally

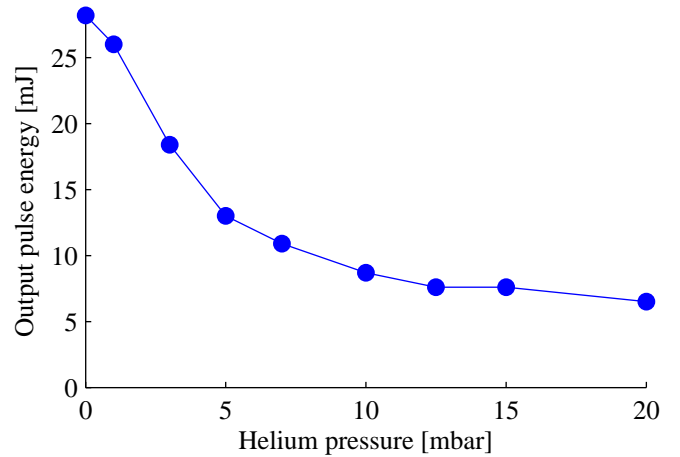


Figure 5. Output pulse energy as a function of the helium pressure for incident pulse energies of 75 mJ.

narrow signal attributed to short trajectories. This harmonic shape is typical for low intensity plateau harmonics [20, 21].

To efficiently generate harmonics at high intensity, we

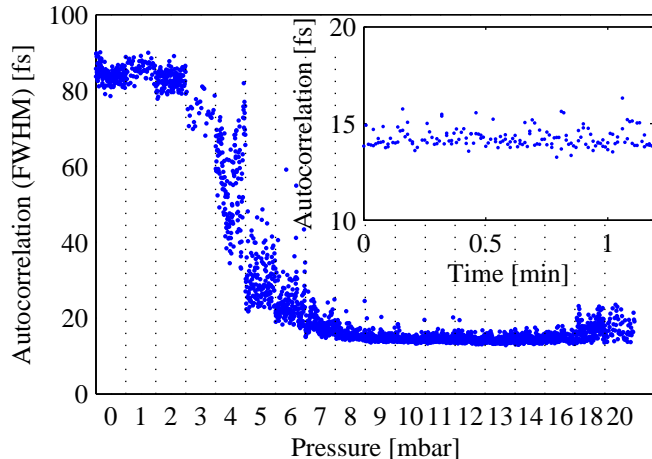


Figure 6. Helium pressure dependence of the pulse autocorrelation FWHM showing a single shot real-time response. The input pulse energy before the capillary was 75 mJ. Inset shows the pulse duration stability at 10 mbar for a time interval of 1 minute.

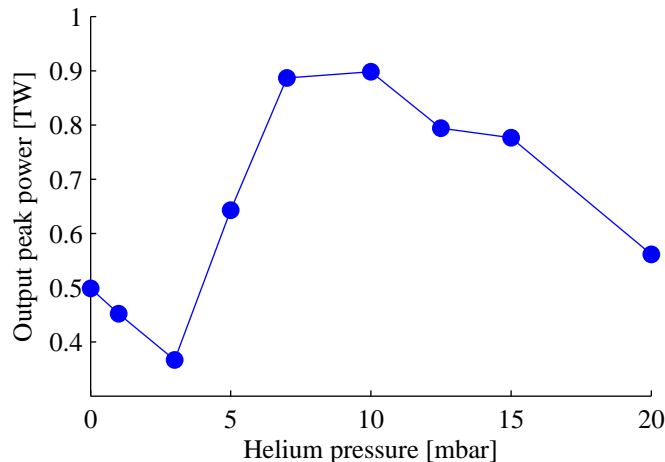


Figure 7. Peak power of output pulses as a function of helium pressure in the capillary. Average values of autocorrelation for given pressures from figure 6 were used and deconvolved by a factor of 1.49.

set the beam size to 12 mm before focusing and approach the beam to the gas jet as close as possible giving the medium length of about 0.7 mm with a high gas density. In these conditions and with 55 fs pulse duration, the intensity at the target reaches $2.5 \times 10^{14} \text{ Wcm}^{-2}$ (figure 8 (b)). Compared to the low intensity case (figure 8 (a)), the signal is increased and the harmonic shape changes dramatically. Long trajectory ellipses are so divergent that their intensity is small compared to the short trajectory signal and they can be barely seen. Short trajectories are brighter than in the low intensity case, spectrally larger and blue-shifted. Spectral symmetry is no longer present and harmonic are asymmetric. This asymmetry is due to argon ionization that favors HHG in the pulse

rising front where the harmonics are blue-shifted. Note, that in contrast with the low intensity case on fig. 8 (a), only the plateau harmonics are presented on figure 8 (b) - (f) to provide better resolution of the spectrograms.

Shorter driving pulses would produce shorter XUV pulses. As the duration of the IR pulse can be changed under vacuum by controlling the helium pressure in the capillary, we performed a study of helium-pressure dependent HHG (figure 8). Note that when the helium pressure is changed, the central wavelength of the driving pulse changes and therefore the harmonic central wavelength is modified as well.

The study is performed for helium pressure of 2, 4, 6 and 8 mbar in the capillary and corresponding XUV spectra shown on figure 8 (c), (d), (e) and (f) respectively. At a given driving intensity, controlling the helium pressure in the capillary is sufficient to tune the driving pulses duration. Therefore other experimental parameters than helium pressure are the same as for figure 8 (b).

One of the most significant change of XUV radiation is the spectral width of the detected harmonics. It increases with pressure and at 8 mbar of helium in the capillary (figure 8 (f)) the spectral width of individual harmonics is so large that even the harmonics spectra overlap each other and create XUV quasi-continuum. The spectral width of harmonics is due to two phenomena: spectral width of the driving infrared pulse and a blue shift during HHG that is due to ionization of the argon gas (ionization-induced blue shift) leading to a confinement of the emission in the pulse rising front [18].

As shown on figure 2, the spectral width of the infrared pulses increases with the helium pressure generating directly large spectral width of the harmonics. However, the infrared pulse spectral width making less than 1/7 of the central photon energy can not explain XUV quasi-continuum.

So the main phenomenon imposing the harmonic spectral width is the XUV blue shift caused by the intensity dependent phase αI_{IR} of the XUV emission and causing the photon energy linear dependence on the $\alpha \frac{dI_{IR}}{dt}$ (where α denotes the harmonic dipole phase) and confinement of the emission in the rising part of the pulse. For high energy ultra-short pulses generated via our post-compression technique, the time derivative of the intensity became high enough to shift the photon energy close to one harmonic creating the XUV quasi-continuum even by considering only the short path contribution (low value of α). This is therefore a second indication that the high energy pulses are very short in the interaction region and can efficiently be used for strong-field physics.

Emission of isolated attosecond pulses confined by ionization gating could also explain this broadening but the existence of spatio-spectral structures in the far field contradicts this option. Clearly distinguishable spatio-spectral structures in XUV spatially-resolved spectra can be seen on figures 8 (e) and (f). Those structures are robust and similar from one harmonic to the other. Indeed, the robustness against medium length and the ar-

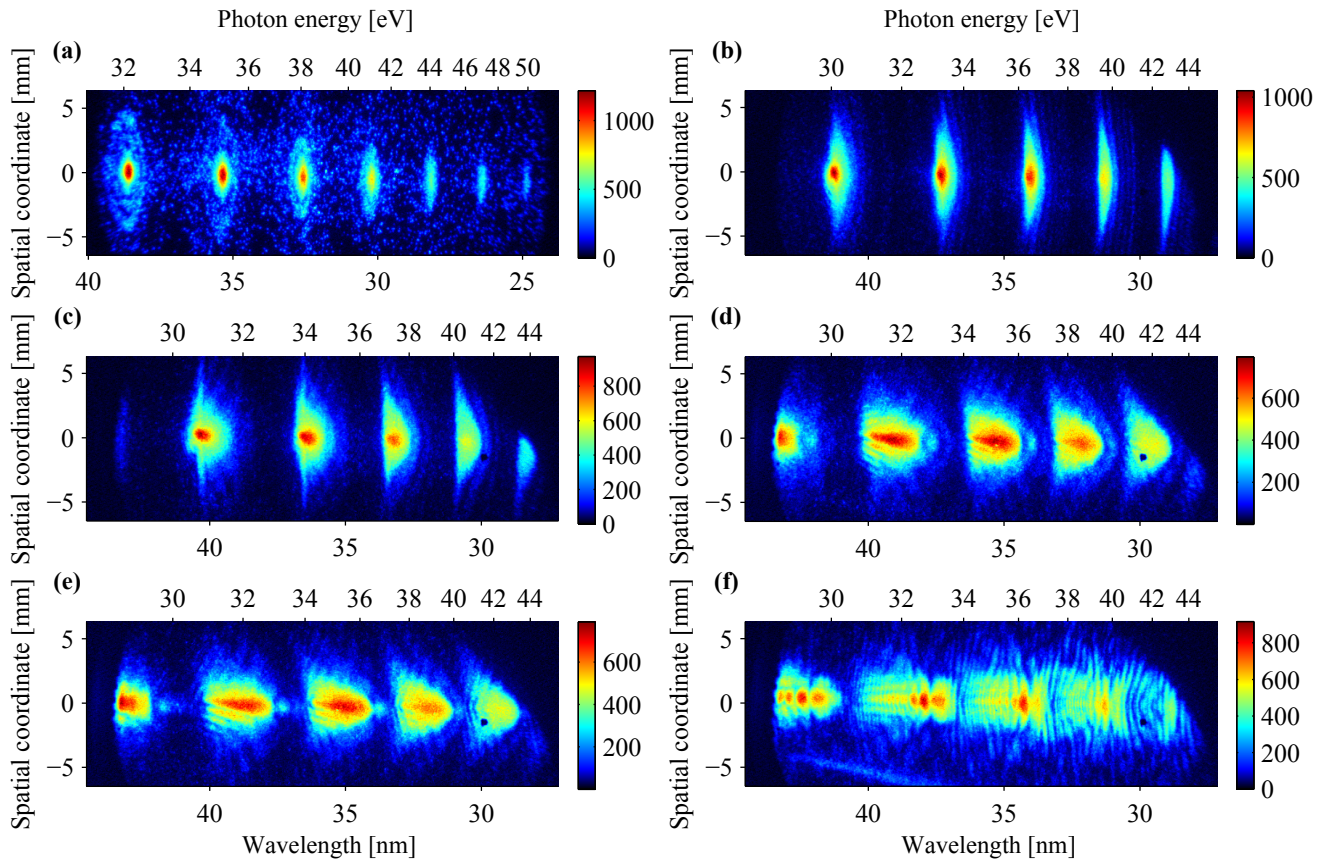


Figure 8. (color online) High harmonic single-shot spatially and spectrally resolved spectra. Before focusing post-compressed pulses were clipped to (a) 10mm (b) - (f) 12 mm. Argon gas jet (4.5 Bar of backing pressure, 250 μm of the valve diameter) 58.5 mm in front of the focus i.e. in the converging beam was used for HHG. The medium length is estimated to 0.7 mm. The focal length of the mirror is 2 meters. The corresponding helium pressure in the capillary is (a) 0 mbar, (b) 0 mbar, (c) 2 mbar, (d) 4 mbar (e) 6 mbar and (f) 8 mbar respectively. Note that the presented spectral window of (a) is different than in cases (b) - (f).

gon pressure (not shown in this paper) suggest that they cannot be explained by phase matching consideration but rather from the spatial coherence of the XUV emission. Precise modeling and explanation of the structures is presented in detail in [18].

IV. CONCLUSION AND PERSPECTIVES

We have demonstrated a TW level 10 Hz laser source with pulse duration adjustable between 55 and 9 fs with good spatial profile. The spectral broadening is achieved via helium ionization in a capillary and the generated pulses are re-compressible close to the Fourier transform limit. We describe how the pulse duration and the output pulse energy can be controlled while preserving the peak power in a large range of parameters. At 10 mbar of helium pressure, we are able to produce pulses of 8.9 fs and 8.7 mJ with a good shot to shot stability on the post-compressed pulse duration (3.4 % RMS). Results are in good agreement with 3D simulations [16, 17].

We performed high harmonic generation in argon gas

jet with these post-compressed TW pulses. The XUV spectra were acquired on a single-shot basis with both spatial and spectral resolution that allow to observe clear spatio-spectral structures. Moreover, when the generating IR pulses are below 10 fs the XUV emission became spectrally quasi-continuous. It can locally support single attosecond pulse generation in the generating medium but the structures that we observe in the far field are strong indications that the macroscopic emission is longer.

In the future, temporal measurement will be implemented to characterize the XUV radiation but its spatio-temporal inhomogeneity will have to be considered. The single shot spectrally resolved XUV characterization can be also coupled with spatial shaping of the driving beam [19, 22, 23] or with gating techniques [24–27] to improve the understanding of the strong spatio-temporal coupling that can occur in the HHG process. This point will get increasingly important with the effort which is currently devoted to develop higher pulse energy driver laser sources.

ACKNOWLEDGMENTS

This work was funded by the CNRS (Pics No PICS06038), the RFBR (grant No 12-02-91059-NCNI a), the European commission (EU program Laserlab Europe II and III with GA-228334 and GA-284464), the ANR (ATTOWAVE ANR-09- BLAN-0031-02), the region

Aquitaine (COLA2 09010502 and NASA 20101304005) and the French National Research Agency (ANR) in the frame of the Investments for the future Programme IdEx Bordeaux—LAPHIA (ANR-10-IDEX-03-02). We also acknowledge our colleagues from CELIA including Yann Mairesse for fruitful discussions.

-
- [1] F. Krausz and M. Ivanov, ‘Attosecond physics’, *Review of Modern Physics* **81**, 163–234 (2009).
- [2] G. Sansone, L. Poletto, and M. Nisoli, ‘High-energy attosecond light sources’, *Nature Photonics* **5**, 655–663 (2011).
- [3] F. Tavella, Y. Nomura, L. Veisz, V. Pervak, A. Marcinkevičius, and F. Krausz, ‘Dispersion management for a sub-10-fs, 10 tw optical parametric chirped-pulse amplifier’, *Optics Letters* **32**, 2227–2229 (2007).
- [4] L. Veisz, D. Rivas, G. Marcus, X. Gu, D. Cardenas, J. Mikhailova, A. Buck, T. Wittmann, C. Sears, S. Chou, J. Xu, G. Ma, D. Herrmann, O. Razskazovskaya, V. Pervak, and F. Krausz, ‘Generation and applications of sub-5-fs multi-10-tw light pulses’, *Pacific Rim Conference on Lasers and Electro-Optics, CLEO - Technical Digest* p. 6600068 (2013).
- [5] S. Bohman, A. Suda, T. Kanai, S. Yamaguchi, and K. Midorikawa, ‘Generation of 5.0 fs, 5.0 mj pulses at 1 khz using hollow-fiber pulse compression’, *Optics Letters* **35**, 1887–1889 (2010).
- [6] F. Böhle, M. Kretschmar, A. Jullien, M. Kovacs, M. Miranda, R. Romero, H. Crespo, U. Morgner, P. Simon, R. Lopez-Martens, and T. Nagy, ‘Compression of cep-stable multi-mj laser pulses down to 4 fs in long hollow fibers’, *Laser Physics Letters* **11**, 095401 (2014).
- [7] S. Akturk, C. L. Arnold, B. Zhou, and A. Mysyrowicz, ‘High-energy ultrashort laser pulse compression in hollow planar waveguides’, *Optics Letters* **34**, 1462–1464 (2009).
- [8] S. Chen, A. Jarnac, A. Houard, Y. Liu, C. Arnold, B. Zhou, B. Forestier, B. Prade, and A. Mysyrowicz, ‘Compression of high-energy ultrashort laser pulses through an argon-filled tapered planar waveguide’, *Journal of the Optical Society of America B: Optical Physics* **28**, 1009–1012 (2011).
- [9] C. P. Hauri, A. Guandalini, P. Eckle, W. Kornelis, J. Biegert, and U. Keller, ‘Generation of intense few-cycle laser pulses through filamentation - parameter dependence’, *Optics Express* **13**, 7541–7547 (2005).
- [10] O. Varela, A. Zaïr, J. Román, B. Alonso, I. Sola, C. Prieto, and L. Roso, ‘Above-millijoule super-continuum generation using polarisation dependent filamentation in atoms and molecules’, *Optics Express* **17**, 3630–3639 (2009).
- [11] B. Alonso, O. Varela, I. Sola, J. San Román, A. Zaïr, C. Méndez, and L. Roso, ‘Energy scaling-up of stable single filament’, *Applied Physics B: Lasers and Optics* **101**, 15–22 (2010).
- [12] P. Heissler, R. Hörlein, J. M. Mikhailova, L. Waldecker, P. Tzallas, A. Buck, K. Schmid, C. M. S. Sears, F. Krausz, L. Veisz, M. Zepf, and G. D. Tsakiris, ‘Few-cycle driven relativistically oscillating plasma mirrors: A source of intense isolated attosecond pulses’, *Physical Review Letters* **108**, 235003 (2012).
- [13] C. Fourcade-Dutin, A. Dubrouil, S. Petit, E. Mével, E. Constant, and D. Descamps, ‘Post-compression of high-energy femtosecond pulses using gas ionization’, *Optics Letters* **35**, 253–255 (2010).
- [14] E. Marcatili and R. Schmelzter, ‘Hollow metallic + dielectric waveguides for long distance optical transmission + lasers’, *Bell System Technical Journal* **43**, 1783 (1964).
- [15] G. Tempea and T. Brabec, ‘Theory of self-focusing in a hollow waveguide’, *Optics Letters* **23**, 762–764 (1998).
- [16] T. Auguste, O. Gobert, C. F. Dutin, A. Dubrouil, E. Mével, E. Petit, S. Constant, and D. Descamps, ‘Application of optical-field-ionization-induced spectral broadening in helium gas to the postcompression of high-energy femtosecond laser pulses’, *Journal of the Optical Society of America B: Optical Physics* **29**, 1277–1286 (2012).
- [17] T. Auguste, C. Fourcade Dutin, A. Dubrouil, O. Gobert, O. Hort, E. Mével, S. Petit, E. Constant, and D. Descamps, ‘High-energy femtosecond laser pulse compression in single- and multi-ionization regime of rare gases: Experiment versus theory’, *Applied Physics B: Lasers and Optics* **111**, 75–87 (2013).
- [18] A. Dubrouil, O. Hort, F. Catoire, D. Descamps, S. Petit, E. Mével, V. Strelkov, and E. Constant, ‘Spatio-spectral structures in high-order harmonic beams generated with terawatt 10-fs pulses’, *Nature Communications* **5** (2014).
- [19] A. Dubrouil, Y. Mairesse, B. Fabre, D. Descamps, S. Petit, E. Mével, and E. Constant, ‘Controlling high harmonics generation by spatial shaping of high-energy femtosecond beam’, *Optics Letters* **36**, 2486–2488 (2011).
- [20] A. Zaïr, M. Holler, A. Guandalini, F. Schapper, J. Biegert, L. Gallmann, U. Keller, A. S. Wyatt, A. Monmayrant, I. A. Walmsley, E. Cormier, T. Auguste, J. P. Caumes, and P. Salières, ‘Quantum path interferences in high-order harmonic generation’, *Physical Review Letters* **100**, 143902 (2008).
- [21] C. M. Heyl, J. Gädde, U. Höfer, and A. L’Huillier, ‘Spectrally resolved maker fringes in high-order harmonic generation’, *Physical Review Letters* **107**, 033903 (2011).
- [22] V. Strelkov, E. Mével, and E. Constant, ‘Isolated attosecond pulse generated by spatial shaping of femtosecond laser beam’, *European Physical Journal: Special Topics* **175**, 15–20 (2009).
- [23] E. Constant, A. Dubrouil, O. Hort, S. Petit, D. Descamps, and E. Mével, ‘Spatial shaping of intense femtosecond beams for the generation of high-energy attosecond pulses’, *Journal of Physics B: Atomic, Molecular and Optical Physics* **45**, 074018 (2012).
- [24] I. Sola, E. Mével, L. Elouga, E. Constant, V. Strelkov,

- L. Poletto, P. Villoresi, E. Benedetti, J.-P. Caumes, S. Stagira, C. Vozzi, G. Sansone, and M. Nisoli, 'Controlling attosecond electron dynamics by phase-stabilized polarization gating', *Nature Physics* **2**, 319–322 (2006).
- [25] X. Feng, S. Gilbertson, H. Mashiko, H. Wang, S. D. Khan, M. Chini, Y. Wu, K. Zhao, and Z. Chang, 'Generation of isolated attosecond pulses with 20 to 28 femtosecond lasers', *Physical Review Letters* **103**, 183901 (2009).
- [26] M. J. Abel, T. Pfeifer, P. M. Nagel, W. Boutu, M. J. Bell, C. P. Steiner, D. M. Neumark, and S. R. Leone, 'Isolated attosecond pulses from ionization gating of high-harmonic emission', *Chemical Physics* **366**, 9–14 (2009). *Attosecond Molecular Dynamics*.
- [27] K. Kim, C. Zhang, T. Ruchon, J.-F. Hergott, T. Auguste, D. Villeneuve, P. Corkum, and F. Quéré, 'Photonic streaking of attosecond pulse trains', *Nature Photonics* **7**, 651–656 (2013).